

Article

The Influence of Cr Addition on the Microstructure and Mechanical Properties of Fe-25Mn-10Al-1.2C Lightweight Steel

Rui Bai *, Yunfei Du, Xiuli He and Yaqin Zhang

Department of Mechanical Engineering, Taiyuan Institute of Technology, Taiyuan 030008, China; duyunfei@tit.edu.cn (Y.D.); hexiuli@tit.edu.cn (X.H.); jxx@tit.edu.cn (Y.Z.)

* Correspondence: bair@tit.edu.cn; Tel.: +86-189-3511-8043

Abstract: The influence of Cr addition on the microstructure and tensile properties of Fe-25Mn-10Al-1.2C lightweight steel was investigated. The characteristics of the microstructures and deformation behavior were carried out through X-ray diffraction (XRD), scanning electron microscopy (SEM), transmission electron microscopy (TEM), electron backscatter diffraction (EBSD), and room temperature tensile testing. Fe-20Mn-12Al-1.5C steel without Cr exhibited a fully austenitic single phase. With the addition of Cr, the volume fraction of ferrite continuously increased. When the content of Cr exceeded 5 wt%, the precipitation of Cr₇C₃ carbides was observed. In the steel with 5 wt% Cr, the quantity of κ carbides remarkably decreased, indicating that the addition of 5 wt% Cr significantly inhibited the nucleation of κ -carbides. As the Cr content increases from 0 wt% to 5 wt%, the austenite grain sizes were 8.8 μm and 2.5 μm , respectively, demonstrating that Cr alloying is an effective method of grain refinement. Tensile strength increased slightly while elongation decreased with increasing Cr content. As the Cr content exceeded 5 wt%, the yield strength increased but the elongation drastically decreased. The steel with 2.5 wt% Cr achieved a synergistic improvement in strength and ductility, exhibiting the best tensile performance.

Keywords: lightweight steels; Cr content; κ -carbides; grain refinement; tensile properties



Citation: Bai, R.; Du, Y.; He, X.; Zhang, Y. The Influence of Cr Addition on the Microstructure and Mechanical Properties of Fe-25Mn-10Al-1.2C Lightweight Steel. *Metals* **2024**, *14*, 687. <https://doi.org/10.3390/met14060687>

Academic Editor: Seok Su Sohn

Received: 1 May 2024

Revised: 30 May 2024

Accepted: 7 June 2024

Published: 10 June 2024



Copyright: © 2024 by the authors. Licensee MDPI, Basel, Switzerland. This article is an open access article distributed under the terms and conditions of the Creative Commons Attribution (CC BY) license (<https://creativecommons.org/licenses/by/4.0/>).

1. Introduction

The need to reduce vehicle weight in the automobile industry is driven by the goal of improving fuel efficiency and reducing carbon dioxide emissions. In the research of developing high-strength and lightweight steels, Fe-Mn-Al-C steels have gained attention for their advantages by combining excellent mechanical properties with a low density [1–4]. These steels can be categorized into fully ferritic, fully austenitic, ferrite-based duplex, and austenite-based duplex depending on their constitution phase [5–8]. Their unique properties make them suitable for various industrial applications. Austenitic or austenite-based duplex steels, containing a higher Al content (5~12%) and higher C content (0.5~2.0%), consist of an austenite matrix phase, ferrite phase, and nano-sized κ -carbide [9–12]. The high content of alloying elements contributes to solid solution strengthening, and the high aluminum content contributes to precipitation hardening of nano-scale particles, resulting in excellent mechanical properties. The high stacking fault energy of these steels causes deformation mechanisms like shear band-induced plasticity (SIP), microband-induced plasticity (MBIP), and slip band refinement-induced plasticity (SRIP) [13–17].

Several studies indicate that the addition of a chromium alloying element has a positive effect on improving the corrosion resistance, high-temperature oxidation performance, environmental brittleness, and tear resistance of Fe-Mn-Al-C steels [18–22]. Additionally, chromium alloying has been found to have a significant impact on phase transformation, enlarging the austenite and ferrite two-phase region in phase diagrams and promoting the precipitation of ordered phases such as B2 and D0₃ [23–25]. Recent studies have shown that the appropriate addition of chromium can achieve the balance of strength and

ductility of lightweight Fe-Mn-Al-C steels, providing a promising avenue for optimizing the mechanical properties of these steels [26–29]. However, the research on the effects of chromium on the mechanical properties and phase transformation of these alloys is still relatively limited. The understanding of how Cr addition precisely suppresses the precipitation of κ -carbides within austenite grains and along grain boundaries in Fe–Mn–Al–C steels remains inadequate.

In summary, this study aims to reveal comprehensive influence of different Cr content (2.5 wt%, 5 wt%, 7.5 wt%, and 10 wt%) on the microstructures, mechanical properties, and deformation behavior of austenite-based lightweight Fe-25Mn-10Al-1.2C steel. In addition, the alloying role of Cr in regulating κ -carbide precipitation was explored, and the effect of Cr addition on the recrystallization behavior was also discussed. This study systematically explores the complex relationships between alloy composition, heat treatment processes, microstructural evolution, and mechanical properties. The finding could contribute to the optimization of alloy designs for lightweight steel applications, and the balancing of strength and ductility by the addition of chromium.

2. Materials and Methods

The Fe-24.6Mn-10.4Al-1.2C-xCr ($x = 0, 2.5, 5, 7.5, \text{ and } 10 \text{ wt\%}$, denoted as A, B, C, D, and E, respectively) steel ingots were prepared by using vacuum induction melting and casting into a copper mold for rapid cooling, with dimensions of $100 \text{ mm} \times 50 \text{ mm} \times 10 \text{ mm}$. The chemical compositions of the steels were measured using chemical analysis. The average density of the steels was measured based on the Archimedean method. The measured compositions and densities are listed in Table 1. The ingots were homogenized at $1150 \text{ }^\circ\text{C}$ for 4 h and air cooled to ambient temperature. Subsequently, solid solution treatment was carried out at $1050 \text{ }^\circ\text{C}$ for 1 h and water quenched. After solid solution treatment, the samples were cold rolled with a thickness reduction of 78%, and then subjected to recrystallization annealing at $950 \text{ }^\circ\text{C}$ for 10 min.

Table 1. Chemical compositions (wt%) and densities of the experimental steels.

Steels	Fe	Mn	Al	C	Cr	Density/g·cm ^{−3}
A(0Cr)	Bal.	24.6	10.4	1.22	0	6.63
B(2.5Cr)	Bal.	25.2	10.2	1.24	2.47	6.64
C(5Cr)	Bal.	24.8	9.8	1.19	5.15	6.66
D(7.5Cr)	Bal.	25.4	10.3	1.17	7.53	6.59
E(10Cr)	Bal.	24.9	9.7	1.23	10.12	6.65

Phase identification was performed using Rigaku D/max 2550 X-ray diffractometer (XRD, Rigaku Corporation, Tokyo, Japan). The measurement parameters were Cu-K α Radiation, the working voltage 40 kV, the scanning angle range $20\text{--}100^\circ$ and the speed $4^\circ/\text{min}$. The ZEISS SUPRA55 scanning electron microscope (SEM, Carl Zeiss AG, Oberkochen, Germany) equipped with an energy dispersive spectrometer (EDS, Thermo Fisher Scientific Inc., Waltham, USA) was used for the characterization of microstructure and the determination of phase composition. The samples for SEM were prepared by mechanical polishing and then etched in 94% ethanol acetic acid and 6% nitric acid solution. The analysis of grain size distribution was conducted by electron backscatter diffraction (EBSD, Oxford Instruments, Oxford, UK). The samples for EBSD were prepared by electrolytic polishing, with an electrolyte solution of 90% ethanol and 10% perchloric acid, and a working voltage of 20 V.

The precipitation of κ -carbides was observed using JEM 2100F transmission electron microscopy (TEM, JEOL Ltd., Tokyo, Japan) at a working voltage of 200 kV. The samples for TEM were prepared by double spray electrolytic polishing using a solution of 95% acetic acid and 5% perchloric acid at a voltage of 20 V and a temperature of $-25 \text{ }^\circ\text{C}$. The tensile test was conducted using the CMT 4105 testing machine (Sansi Testing Instrument Ltd., Shenzhen, China) with a constant strain rate of $1 \times 10^{-3} \text{ s}^{-1}$. The plate-shaped specimens

were machined with a thickness of 2 mm, a width of 5 mm, a gauge length of 20 mm, and a total length of 55 mm.

3. Results and Discussion

3.1. Microstructure Evolution

The XRD patterns of six as-cast samples are shown in Figure 1. Sample A without Cr exhibited a fully austenitic single phase. With the increasing of Cr content, the diffraction peaks of the ferritic phase continuously increased in intensity. This indicates that Cr addition enhanced the phase transformation of austenite to ferrite. In particular, at a critical value of 5% Cr content, a marked change in the phase structure was observed. As shown in Figure 1b, there were obvious characteristic diffraction peaks in the Cr_7C_3 phase in samples D and E, identified as the (202) crystal plane at 42.8° and the (600) crystal plane at 45.1° , respectively. And there was a clear diffraction peak in the B2 or D0_3 phase on the (200) crystal plane at 30.8° in E. It indicates that when the Cr content exceeded 5 wt%, there was significant promotion of the formation of ferrite, the precipitation of Cr carbides and other ordered structural phases.

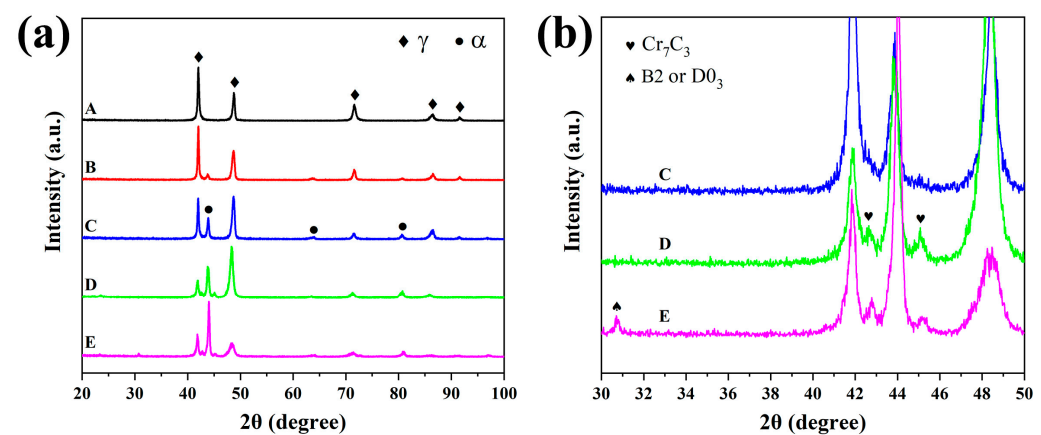


Figure 1. XRD patterns of the samples in the as-cast state; (a) the curves of all samples at $20\text{--}100^\circ$; (b) the amplified curves of samples C, D, and E at $30\text{--}50^\circ$.

The phase transformation of Fe-8.7Al-28.3Mn-1C-5.5Cr steel [24] aged at $700\text{--}800^\circ\text{C}$ after solution treatment was investigated. Phase transformation from γ to $(\gamma + \text{Cr}_7\text{C}_3)$ occurred within the austenite matrix, and the transformation from γ to $(\text{D0}_3 + \text{Cr}_7\text{C}_3)$ was observed at the grain boundaries. The influence of Cr content on the high-temperature microstructure of the Fe-9Al-30Mn-xC-yCr steels [25] annealed at $950\text{--}1100^\circ\text{C}$ was investigated using TEM. It was found that with increasing Cr content, the phase transformation sequence within the α phase was identified as $\alpha + \text{B2} \rightarrow \alpha + \text{B2} + \text{D0}_3 \rightarrow \alpha + \text{D0}_3$. An increase of C or Cr content promoted the formation of Cr_7C_3 .

The Fe-20Mn-12Al-1.5C lightweight steels [26] with different Cr contents, annealed at 1050°C , were investigated. XRD results indicated that the alloys with less than 5 wt% Cr consisted mainly of a large amount of austenite, with small amounts of κ -carbides and ferrite or a D0_3 phase. The alloys with Cr contents exceeding 5 wt% exhibited the presence of a new phase, Cr_7C_3 carbide, and more D0_3 phases. The Fe-20Mn-9Al-1.2C-xCr steels [27,28], prepared by near-rapid solidification, consisted primarily of austenite and ferrite phases. With an increasing Cr content, the intensity of characteristic peaks of δ -ferrite increased. The addition of Cr promoted the transformation from δ -ferrite to an ordered D0_3 phase, with a significantly enhanced diffraction peak intensity of the ordered D0_3 phase after annealing at 600°C . The Fe-20Mn-11Al-1.8C-5Cr quinary alloy [29], synthesized at 1373 K using Spark Plasma Sintering (SPS), contained FCC austenite, L1_2 -type κ -carbides, and orthorhombic Cr_7C_3 carbides according to XRD patterns.

In the binary Fe-Al phase diagram, when the Al atom fraction is higher than 20%, the disordered structure of the BCC will transition to ordering, forming a stable FeAl phase with a B2 structure or a Fe₃Al phase with a D0₃ structure. Due to the higher content of aluminum in Fe-Mn-Al-C lightweight steels, the B2 ordered phase and D0₃ ordered phase are typically formed within the ferrite. These ordered phase structures can be observed from electron diffraction patterns by TEM. With the addition of Cr, due to the negative binary enthalpy of mixing between C and Cr (−61 kJ/mol), there is a strong tendency for bonding and forming compounds such as Cr₇C₃, Cr₂₃C₆, and Cr₃C₂, and the Gibbs free energy of these Cr carbides is relatively low. These intermetallic compounds are typically brittle and hard, often significantly enhancing the material's strength while affecting its plasticity and deformation ability.

The SEM microstructure images of the as-cast samples (B, C, D, and E) are shown in Figure 2. With the increase in Cr content, the volume fractions of the ferrite continuously increased, which were 2.9%, 18.7%, 34.6%, and 67.2%, respectively. This indicates that Cr was an element that promotes the formation of ferrite, and it played a significant role in stabilizing the ferrite phase. The precipitation of the Cr carbide occurred as the addition of Cr content exceeded 5 wt%. A large amount of Cr carbides precipitated from the ferrite matrix. This demonstrates that the addition of Cr both stabilized the ferrite and promoted the formation of Cr carbides.

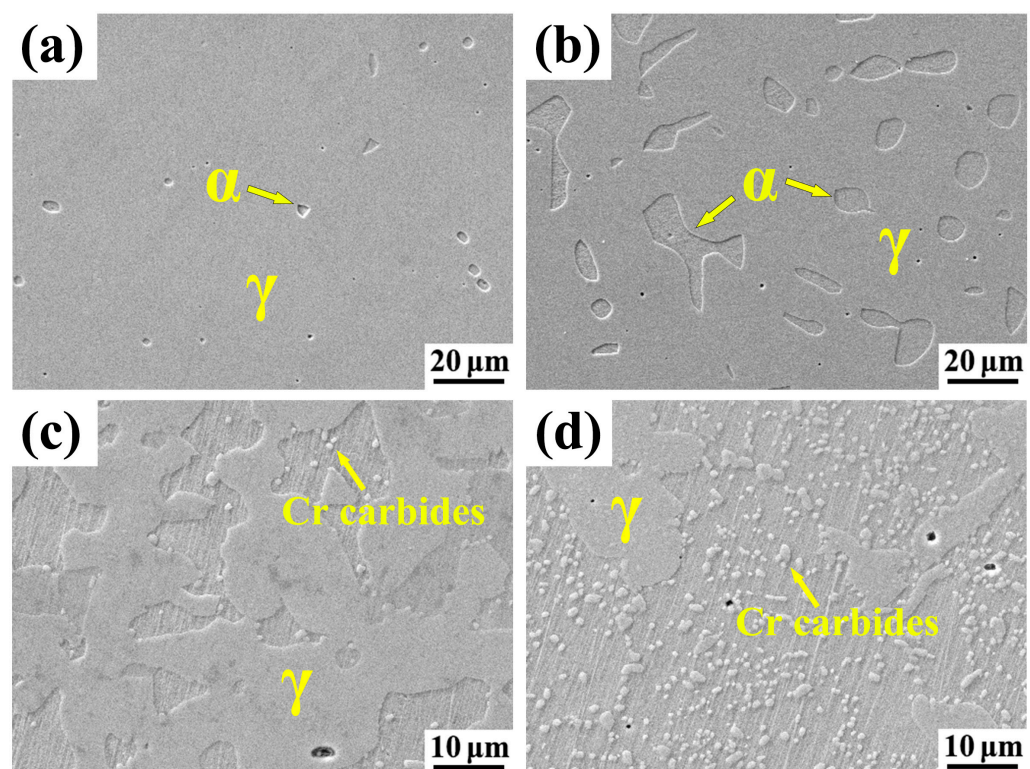


Figure 2. SEM microstructure images of the samples in the as-cast state; (a) B(2.5Cr); (b) C(5Cr); (c) D(7.5Cr); (d) E(10Cr).

The Fe-20Mn-9Al-1.2C-xCr steels [27,28] consisted of a dual-phase microstructure of γ -austenite and δ -ferrite. At different Cr contents of 0%, 3%, 6%, and 9%, the volume fractions of δ -ferrite were 3%, 8%, 17%, and 27%, respectively. The addition of Cr altered the morphology of the ferrite phase from short rod-like to block-like. The Fe-12Mn-9Al-1.4C steel [30] exhibited a ferrite volume fraction of 9%, with the precipitation of granular κ -carbides at austenite grain boundaries. In contrast, the ferrite volume fraction of the steel with 3 wt% Cr addition increased to 13%, with almost no precipitation at austenite grain boundaries.

The high-aluminum Fe-20Mn-12Al-1.5C steel [26] exhibited a complex microstructure due to its high aluminum content, consisting of an austenite matrix, fine κ -carbides within the austenite, coarse κ -carbides at grain boundaries, and a small amount of ferrite. After adding 5.5 wt% Cr, the fraction of ordered $D0_3$ phase increased dramatically and Cr-rich M_7C_3 carbides began to precipitate, while coarse κ -carbides at grain boundaries were eliminated. High-carbon Fe-28Mn-8.5Al-2C steel [31] was a single-phase austenite after high-temperature solution treatment and aging treatment at 800 °C. When the added Cr content was less than 6%, the alloy exhibited a lamellar microstructure of γ/κ . However, when the added Cr content exceeded 6%, abundant Cr_7C_3 carbides formed within the γ matrix, reducing the C content in the matrix and resulting in a decrease in the quantity of κ -carbides. Electron probe microanalysis (EPMA) revealed that Al was almost insoluble in the Cr_7C_3 carbides.

Experimental results from various studies highlight the impact of Cr content on the microstructures and phase compositions of different steels. In the case of the Fe-20Mn-9Al-1.2-xCr steels, increasing the Cr content leads to a higher volume fraction of δ -ferrite, altering its morphology from rod-like to block-like, and promoting the precipitation of Cr carbides. Similarly, the Fe-12Mn-9Al-1.4C steel exhibited increased ferrite volume fraction with Cr addition. Contrastingly, the high-aluminum Fe-20Mn-12Al-1.5C steel displayed a complex microstructure primarily consisting of an austenite matrix and various carbide phases. The addition of Cr resulted in the appearance of an ordered $D0_3$ phase and Cr-rich M_7C_3 carbides while eliminating κ -carbides at grain boundaries. Lastly, in the high-carbon Fe-28Mn-8.5Al-2C steel, increasing the Cr content led to the formation of Cr_7C_3 carbides within the γ matrix, reducing the quantity of κ -carbides. Overall, Cr addition plays a crucial role in stabilizing ferrite, altering the morphology of ferrite, and influencing the precipitation of carbides, with varying effects observed depending on alloy composition and processing conditions.

The SEM-EDX elemental mappings of sample E are shown in Figure 3, revealing the distribution of elements in the precipitates. It can be seen that the granular precipitates were enriched in Cr and C but depleted in Fe and Al, compared with the matrix ferrite phase, and Mn was distributed homogeneously in both phases. It confirms that the precipitates were the Cr carbides, consistent with the phase structure determined by XRD.

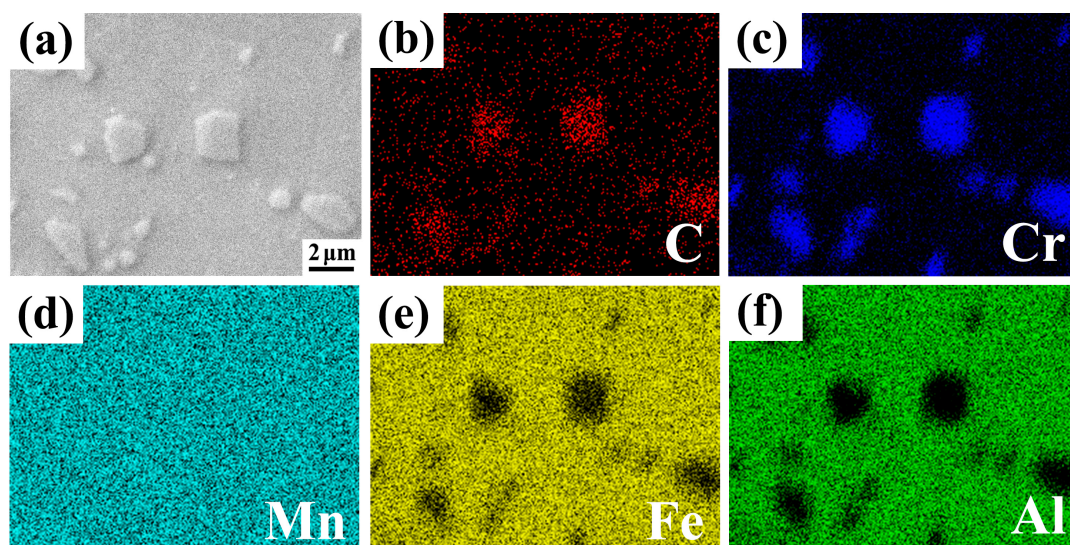


Figure 3. SEM-EDX elemental mapping of sample E; (a) the SEM image and the corresponding EDS elemental maps of (b) C; (c) Cr; (d) Mn; (e) Fe; (f) Al.

3.2. Mechanical Properties and Deformation Behavior

Figure 4a illustrates the engineering stress–strain curves of the samples. The mechanical properties of all the samples are listed in Table 2. The yield strength, tensile strength,

and elongation of sample A was 527 MPa, 708 MPa, and 56.5%, respectively. Sample B exhibited an increase of 32 MPa in yield strength, 65 MPa in tensile strength, and 5% in elongation compared to sample A. The steel with the addition of 2.5% Cr achieved a synergistic improvement in both strength and plasticity. When the content of Cr exceeded 5 wt%, the yield strength significantly increased while the elongation decreased substantially. Sample C showed a yield strength of 585 MPa and an elongation of 21%. Sample E exhibited almost no plasticity, and the strength cannot be further improved. The strength–ductility product, as a comprehensive performance index, characterizing the strength and toughness of metals, is defined as the product of tensile strength and elongation after fracture. The strength–ductility products of sample A and B were 40 GP% and 48 GP%, respectively, higher than the typical TRIP steels (~20 GP%) and close to commercial TWIP steels (~50 GP%).

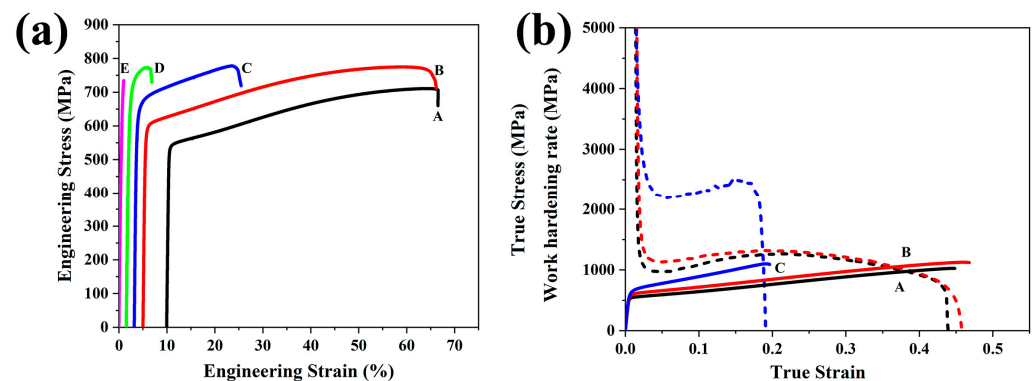


Figure 4. (a) The representative engineering stress–strain curve of all samples at room temperature; (b) The corresponding true stress–strain curves and strain hardening rate curves of samples A, B, and C.

Table 2. Yield strength (YS), ultimate tensile strength (UTS), tension elongation (TE), and product of tensile strength and elongation (UTS*TE) of the experimental steels.

Steels	YS/MPa	UTS/MPa	TE/%	UTS*TE/GPa·%
A(0Cr)	527	708	56.5	40.0
B(2.5Cr)	559	773	61.5	47.5
C(5Cr)	585	775	21.2	16.4
D(7.5Cr)	597	771	5.1	3.9
E(10Cr)	-	732	-	-

Figure 4b shows the corresponding true stress–strain curves and strain hardening rate curves of samples A, B, and C. All samples exhibited extensive strain hardening after yielding. Samples A and B showed similar strain hardening behaviors. The strain hardening rate continuously increased at the early stage of plastic deformation (true strain of ~0.05), reaching the maximum value of 1300 MPa at strain ~0.2, and then decreased, reaching plastic instability at a true strain of ~0.43. At the intersection points of the true stress–true strain curves and the corresponding work hardening rate curves of samples A and B, the range of true strain was approximately 0.36 to 0.38. This indicates that within a wide range of plastic strains, the two steels exhibited the potential for sustained strain strengthening under excellent plasticity. Sample C reached its maximum strain hardening rate at a true strain of ~0.15, with a value of 2490 MPa, followed by a rapid decrease, showing excellent high strain hardening ability within its plastic deformation range.

The Fe-28Mn-9Al-0.8C austenitic steel [32], showing extremely high ductility, achieved a strength–ductility product of 84 GP% and strain hardening rates between 1500 MPa and 2000 MPa. The Fe-28Mn-10Al-1.0C steel [33] was also fully austenitic, exhibiting exceptionally high uniform elongation (85% to 100%) and total elongation (100% to 110%)

at room temperature, with strain hardening rates between 1200 MPa and 1800 MPa. The Fe-27Mn-11.5Al-0.95C dual-phase steel [34] consisted of an austenitic matrix and a small amount of ferrite, showing an excellent combination of high strength and good ductility in the solution-treated state (a strength–ductility product of 46.5 GPa%). The work hardening rate during the continuous hardening stage maintained a constant of approximately 1500 MPa.

Compared to other studies, samples A and B show competitive strength–ductility products, approaching those of commercial TWIP steels. However, they fall short of the extremely high ductility achieved by fully austenitic steels such as the Fe-28Mn-9Al-0.8C and Fe-28Mn-10Al-1.0C steels. Overall, while samples A and B demonstrate promising strength–ductility products and sustained strain strengthening, they exhibit differences in performance compared to fully austenitic steels like those studied in the referenced works. Further exploration of alloying elements and composition optimization could lead to improvements in both strength and ductility for future applications.

Figure 5 illustrates the tensile fracture morphologies of samples A, B, C, and D. A large number of ductile dimples, ranging in size approximately from 1–3 μm , can be observed on the fracture surface of sample A, showing a typical morphology of ductile fracture. Sample B exhibited a fracture surface with smaller and more uniformly distributed dimples, contributing to its excellent tensile property. From the fracture surface of C, it can be observed that the number of ductile dimples has significantly reduced, and there are distinct features of cleavage fracture. This was a mixed-type fracture. There are many macroscopic features of “small facets” on the cleavage fracture surface, as well as some microscopic morphology of “tongue-like patterns”. The fracture morphology of sample D was characterized by a quasi-cleavage fracture. There are many short and curved tearing edges, and a “river pattern” radiating from the crack source to the surrounding area, along with secondary cracks on the fracture surface.

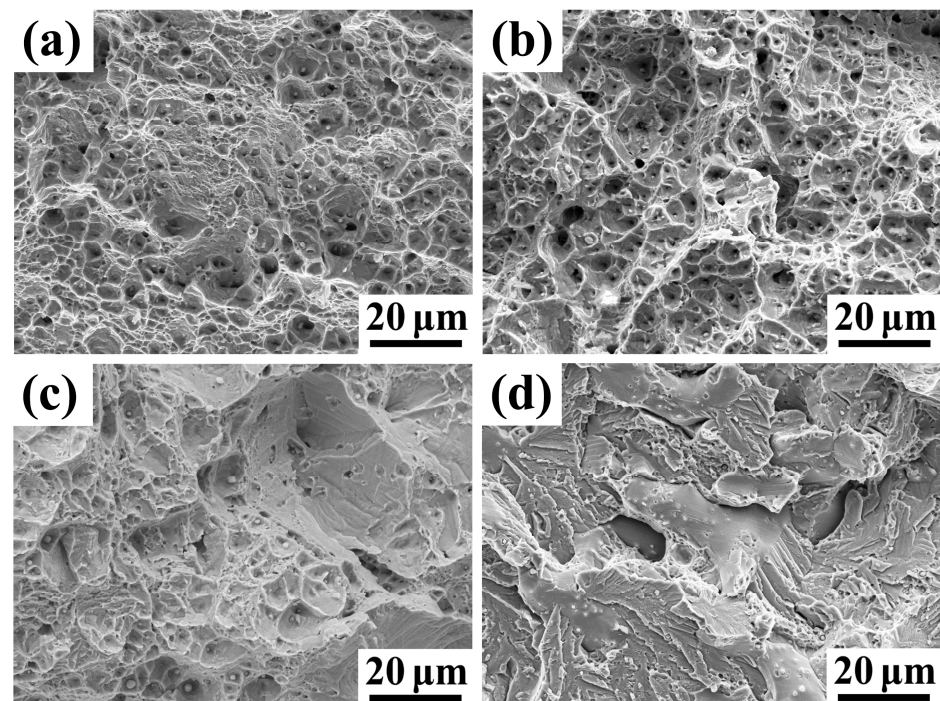


Figure 5. SEM fracture morphologies of the samples in the as-cast state; (a) A(0Cr); (b) B(2.5Cr); (c) C(5Cr); (d) D(7.5Cr).

3.3. Precipitation of Intragranular κ -Carbides

The SEM morphologies of the fracture surfaces in samples A and C are shown in Figure 6. In Figure 6a, it is clearly shown that small κ -carbides existed within the dimples,

with sizes ranging from approximately 100 to 500 nm. During stretching, these κ -carbides exhibited weak bonding with the matrix, leading to their rupture at the interface under external forces, then forming micropores. The κ -carbides had an almost one-to-one correspondence with the dimples, indicating that each κ -carbide serves as a nucleation site for a dimple. The morphology of the dimple region in sample C is illustrated in Figure 6b, showing a significantly lower quantity of κ -carbides. The comparison of results proves that the addition of 5% Cr effectively inhibits the nucleation of κ -carbides.

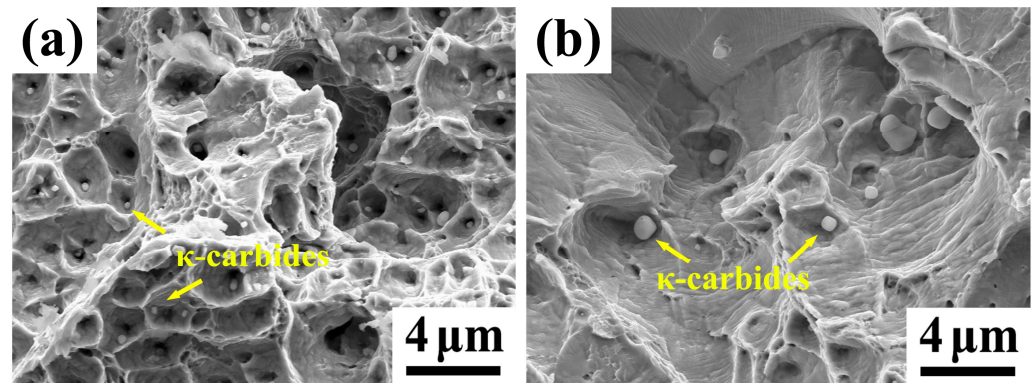


Figure 6. SEM fracture images of the samples in the as-cast state; (a) A(0Cr); (b) B(5Cr).

The dark-field TEM microstructures of the austenite region after solid solution at 1100 °C for samples A and C are shown in Figure 7. In sample A without Cr addition, κ -carbides were uniformly distributed within the austenite matrix, varying in size from large to small, approximately 2 to 20 nm. In contrast, in sample C with a 5 wt% Cr addition, the distribution of κ -carbides was inhomogeneous, with a significant reduction in quantity, and a size mostly smaller than 5 nm. In the Fe-20Mn-12Al-1.5C steel [26] with a 5 wt% Cr addition, the TEM microstructure of the high-temperature homogenized sample revealed that Cr suppresses the precipitation of coarse κ -carbides around the austenite grain boundaries, and the κ -carbides within the austenite become finer. In the Fe-12Mn-9Al-1.4C-3Cr steel [30], in the as-cast state without Cr addition, coarse κ -carbides were observed at the austenite grain boundaries, with an average size of approximately 100 nm, while the average size of internal κ -carbides is about 10 nm. After adding 3 wt% Cr, κ -carbides are almost absent at the austenite grain boundaries, and the average size of internal κ -carbides was around 3 nm.

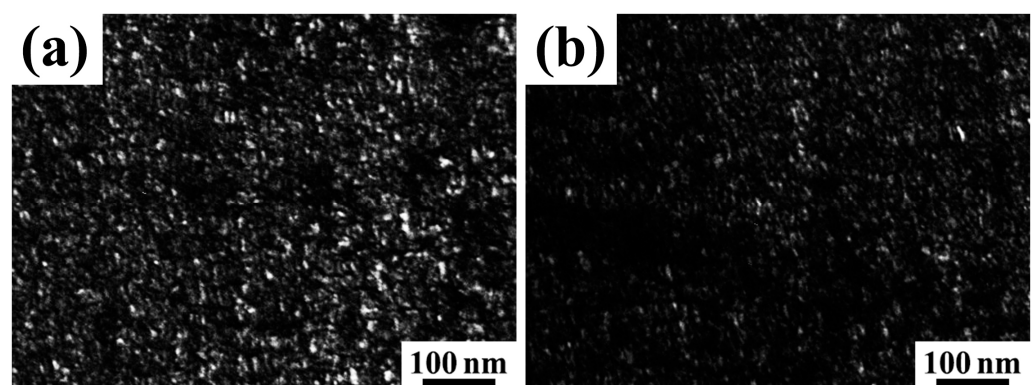


Figure 7. TEM dark-field image of fine κ -carbides in the austenite matrix of the samples in the solid solution state; (a) A(0Cr); (b) C(5Cr).

The effect of Cr content on the intragranular κ -carbide precipitation of the Fe-20Mn-9Al-1.2C steel [35] was investigated. After near-rapid solidification followed by annealing at 600 °C, TEM images of the austenite showed that the volume fraction and average size

of κ -carbides in the steel without Cr were 7% and 8 nm, respectively, while those in the steel with 3 wt% Cr addition decreased to 4% and 4 nm, respectively. Thermodynamic calculations indicated that increasing Cr content narrowed the temperature range of κ -carbide formation. First-principles calculations revealed that Cr atoms in the κ -carbide unit cell tend to occupy Al sites, increasing the formation energy of κ -carbides and making their formation more difficult.

Comparing these results with other authors' findings, the dark-field TEM microstructures in Figure 7 highlighted the impact of Cr on κ -carbide distribution within the austenite matrix. In sample A (without Cr), κ -carbides were uniformly distributed, while sample C (with 5 wt% Cr) showed an inhomogeneous distribution with smaller κ -carbide sizes. This aligns with observations in the Fe-20Mn-12Al-1.5C steel, where 5 wt% Cr addition suppressed coarse κ -carbide precipitation around grain boundaries. In another study on Fe-12Mn-9Al-1.4C-3Cr steel, Cr addition reduced the size of κ -carbides at grain boundaries. Furthermore, investigations on the Fe-20Mn-9Al-1.2C steel revealed that the increase in Cr content decreased the volume fraction of κ -carbide and the size due to the narrowing of temperature range and the increase in formation energy. Overall, the addition of Cr has a notable impact on κ -carbide distribution, size, and formation energy, leading to the improvement of mechanical properties and inhibiting the formation of micropores during stretching.

3.4. Refinement of Austenite Grain

Grain refinement is an important method for improving the strength and hardness of metals. Traditional steels can effectively refine grain size by way of alloying. The samples with different Cr contents were cold rolled with a total reduction rate of 78% after solution treatment, followed by recrystallization annealing at 950 °C. The IPF maps and corresponding grain size distribution maps obtained through EBSD testing are shown in Figure 8. The austenite grain sizes in the samples with a Cr content of 0 wt%, 2.5 wt%, and 5 wt% were 8.8 μm , 4.6 μm , and 2.5 μm , respectively. Sample A, without Cr, was fully recrystallized at 900 °C, while the recrystallization temperature of sample C, containing 5 wt% Cr, increased to 950 °C. On the one hand, the addition of Cr increased the recrystallization temperature. On the other hand, the presence of second-phase ferrite in the structure after adding Cr has a noticeable effect on inhibiting the growth of micron-sized austenite grains. The results indicate that the addition of Cr alloying can reduce the rate of grain growth at high temperatures.

The influence of Mn, C, and Al contents on grain refinement of Fe-(20~35)Mn-(6~12)Al-(0.6~1.5)C steels [36] was investigated. As the Mn content is 20 wt%, the volume fraction of ferrite is 3.3%, and the austenite grain size was 9.9 μm . While the Mn content increased to 30 wt%, the structure became single-phase austenite, with grain sizes of 23.7 μm . With the C content varying from 1 wt% to 1.5 wt%, the matrix structure was austenite, and the grain size changed little, estimated as approximately 23 μm . When the Al content increased from 6 wt% to 10 wt%, there was little change in grain size, decreasing from 34.2 μm to 29.7 μm . While in the steel with 12 wt% Al, containing 3.1% ferrite, the grain size decreased to 12.6 μm . The results indicate that variation in the content of Mn, C, and Al alloy elements has no obvious effects on grain refinement, but the presence of second-phase ferrite can significantly refine the austenite grain. The effect of Mo addition on grain refinement of Fe-30Mn-10.5Al-1.1C steel [37] was investigated. The steel without Mo, annealed at 1050 °C, consisted of austenite and κ -carbides, with a grain size of 104.6 μm . After adding 4 wt% Mo, the grain size decreased to 13.4 μm . The precipitation of Mo-rich M_6C and M_{23}C_6 carbides inhibited the growth of austenite grains, generating remarkable grain refinement. The effect of Cr addition on grain refinement of Fe-20Mn-12Al-1.5C steel [26] annealed at 1050 °C was investigated. In the steel without Cr, the grain size of austenite was 13.7 μm , while in the steels with a 5.5 wt% Cr addition, the grain size is 9.1 μm . The results indicate that the precipitation of κ -carbides and Cr_7C_3 carbides on austenite grain boundaries did not show significant grain refinement effects.

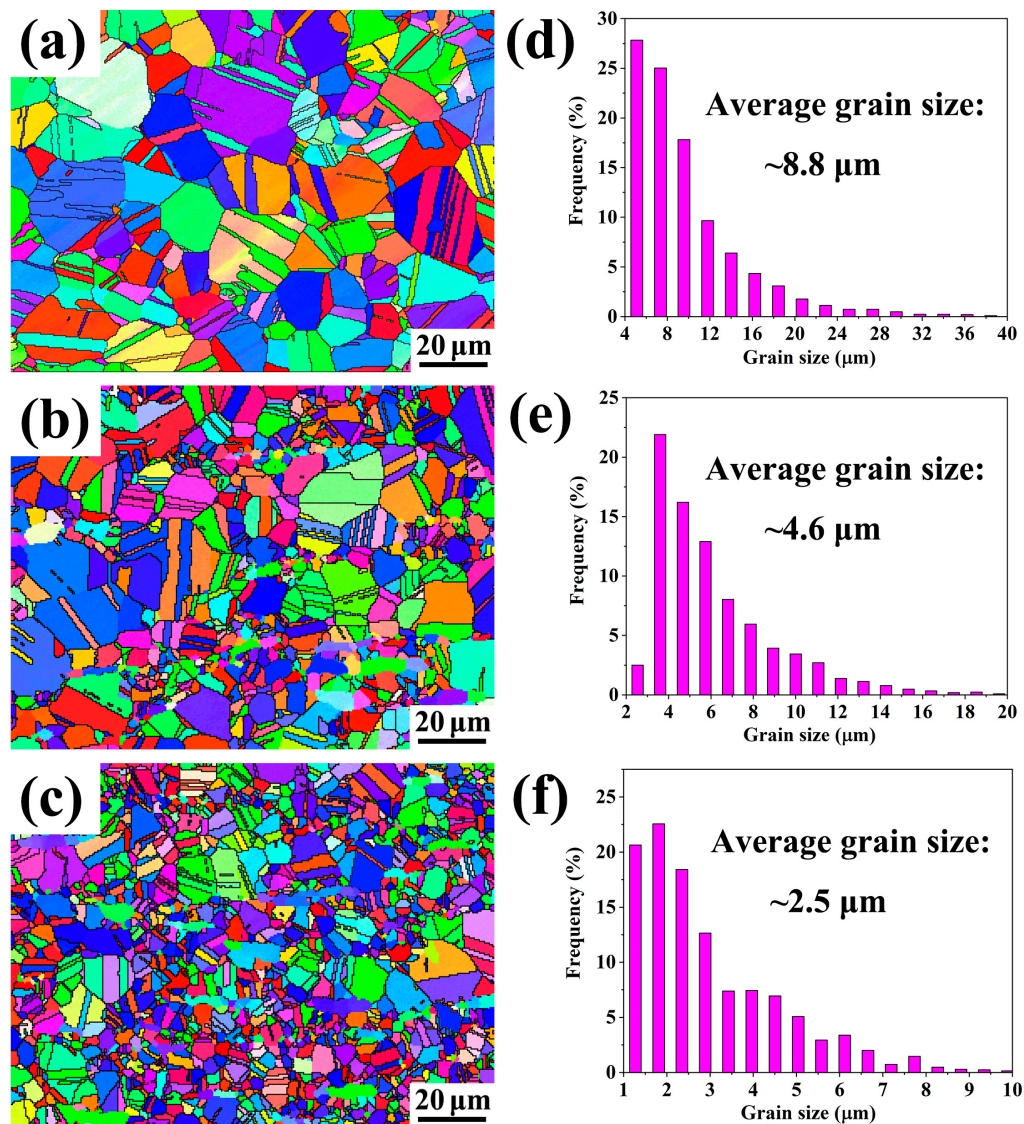


Figure 8. IPF map of the samples after recrystallization and the corresponding distribution of grain size; (a,d) A(0Cr); (b,e) B(2.5Cr); (c,f) C(5Cr).

In summary, Cr addition was found to reduce austenite grain size and increase recrystallization temperature, while the presence of second-phase ferrite and carbides (Mo-rich or Cr-rich) significantly refines the austenite grain. On the other hand, variations in the content of Mn, C, and Al alloy elements had limited effects on grain refinement in the absence of second-phase ferrite.

4. Conclusions

In this study, the influence of Cr alloying on the microstructure evolution and mechanical properties of Fe-25Mn-10Al-1.2C lightweight steel was investigated. Combined with XRD pattern, SEM observation, EBSD characterization, and TEM morphology, the effects of Cr content on the microstructure, κ -carbides, grain size, fracture characteristics, and strain behavior were analyzed. The final conclusions of this paper are as follows:

- (1) The Fe-25Mn-10Al-1.2C steel without Cr contains a fully austenitic single phase. With the addition of Cr content, the volume fraction of ferrite continuously increased. After the Cr content exceeds 5 wt%, the distinct peaks of various ordered structure phases appeared. The Cr-rich phase was confirmed as a Cr_7C_3 carbide through XRD

structure combined with EDS composition. Significant precipitation of Cr_7C_3 carbides was observed when the Cr content exceeded 5 wt%.

- (2) The steel without Cr in the as-cast state contained fine κ -carbides, with sizes ranging from approximately 100 to 500 nm. After solution treatment at 1050 °C, the precipitated phase became finer, with sizes around 2 to 20 nm. In the steel with a 5 wt% Cr content, there were few κ -carbides, and the size mostly was smaller than 5 nm. This indicates that the addition of 5% Cr significantly inhibited the nucleation of κ -carbides and promoted the formation of Cr-rich Cr_7C_3 carbides. After cold rolling, followed by recrystallization annealing at 950 °C, the austenite grain sizes were 8.8 μm , 4.6 μm , and 2.5 μm for Cr contents of 0 wt%, 2.5 wt%, and 5 wt%, respectively. The results indicate that the addition of Cr can play a significant role in refining grain size.
- (3) The tensile strength of the steel without Cr is 708 MPa, with an elongation of 56.5% and a strength–ductility product of 40 GPa%. The addition of 2.5 wt% Cr enhanced both strength and ductility synergistically. When the Cr content exceeds 5 wt%, the strength increased while the elongation decreased due to the precipitation of Cr_7C_3 carbides. The steel with 5 wt% Cr exhibited excellent high-strain hardening ability. As the Cr content increases to 10 wt%, the steel becomes completely brittle.
- (4) The addition of an appropriate Cr content synergistically enhances both strength and ductility, suggesting that this steel could be a promising candidate for applications requiring high strength and good formability. However, the precipitation of Cr_7C_3 carbides at higher Cr contents, which leads to a decrease in ductility, indicates that careful consideration of alloy composition is necessary to avoid brittleness. The findings of this study could also be extended to other alloy systems, contributing to the broader understanding of alloy design and property optimization in lightweight steels.

Author Contributions: Formal analysis, Investigation, Methodology, Writing—original draft, R.B.; Conceptualization, Methodology, Writing—review and editing, Y.D.; Formal analysis, Investigation, X.H.; Writing—review and editing, Y.Z. All authors have read and agreed to the published version of the manuscript.

Funding: This research was funded by the Scientific and Technological Innovation Programs of Higher Education Institutions in Shanxi, China (No. 2022L550), the Free Exploration Natural Science Project of the Basic Research Program of Shanxi Province, China (No. 202203021212212) and the Fundamental Research Program of Shanxi Province, China (No. 202303021212278).

Data Availability Statement: The data that support the findings of this study are available from the corresponding author upon reasonable request.

Acknowledgments: The authors acknowledge Ying Li (Inspection and Testing Center of Shanxi Province, China) for assistance in in tensile performance testing and density measurement.

Conflicts of Interest: The authors declare no conflicts of interest.

References

1. Liu, D.G.; Ding, H.; Han, D.; Cai, M.H. Improvement of the yield strength of Fe-11Mn-xAl-yC medium-Mn lightweight steels by tuning partial recrystallization and intra-granular κ -carbide strengthening. *Mater. Sci. Eng.* **2022**, *833*, 142553. [[CrossRef](#)]
2. Liu, S.; Ge, Y.L.; Liu, H.Y.; Liu, J.Y.; Feng, Y.L.; Chen, C.; Zhang, F.C. Tensile Properties and Microstructure Evolutions of Low-Density Duplex Fe-12Mn-7Al-0.2C-0.6Si Steel. *Materials* **2022**, *15*, 2498. [[CrossRef](#)]
3. Wan, P.; Kang, T.; Li, F.; Gao, P.F.; Zhang, L.; Zhao, Z.Z. Dynamic recrystallization behavior and microstructure evolution of low-density high-strength Fe-Mn-Al-C steel. *J. Mater. Res. Technol.* **2021**, *15*, 1059–1068. [[CrossRef](#)]
4. Piston, M.; Bartlett, L.; Limmer, K.R.; Field, D.M. Microstructural Influence on Mechanical Properties of a Lightweight Ultrahigh Strength Fe-18Mn-10Al-0.9C-5Ni (wt%) Steel. *Metals* **2020**, *10*, 1305. [[CrossRef](#)]
5. Balaško, T.; Šetina, B.B.; Medved, J.; Burja, J. High-Temperature Oxidation Behaviour of Duplex Fe-Mn-Al-Ni-C Lightweight Steel. *Crystals* **2022**, *12*, 957. [[CrossRef](#)]
6. Jung, H.; Lee, G.; Koo, M.; Song, H.; Ko, W.S.; Sohn, S.S. Effects of Mn Segregations on Intergranular Fracture in a Medium-Mn Low-Density Steel. *Steel Res. Int.* **2022**, *94*, 2200240. [[CrossRef](#)]
7. Chen, S.; Rana, R.; Haldar, A.; Ray, R.K. Current state of Fe-Mn-Al-C low density steels. *Prog. Mater. Sci.* **2017**, *89*, 345–391. [[CrossRef](#)]

8. Chen, P.; Li, X.; Yi, H. The κ -Carbides in Low-Density Fe-Mn-Al-C Steels: A Review on Their Structure, Precipitation and Deformation Mechanism. *Metals* **2020**, *10*, 1021. [[CrossRef](#)]
9. Song, H.; Jo, M.; Kim, D.W. Vanadium or copper alloyed duplex lightweight steel with enhanced hydrogen embrittlement resistance at room temperature. *Mater. Sci. Eng.* **2021**, *817*, 141347. [[CrossRef](#)]
10. Huo, Y.T.; He, Y.L.; Zhu, N.Q.; Ding, M.L.; Liu, R.D.; Zhang, Y. Deformation Mechanism Investigation on Low Density 18Mn Steels under Different Solid Solution Treatments. *Metals* **2021**, *11*, 1497. [[CrossRef](#)]
11. Wu, H.; Tan, Y.; Malik, A.; Wang, Y.W.; Naqvi, S.Z.H.; Cheng, H.W.; Tian, J.B.; Meng, X.M. Dynamic Compressive Mechanical Behavior and Microstructure Evolution of Rolled Fe-28Mn-10Al-1.2C Low-Density Steel. *Material* **2022**, *15*, 3550. [[CrossRef](#)] [[PubMed](#)]
12. Ding, H.; Liu, D.; Cai, M.; Zhang, Y. Austenite-Based Fe-Mn-Al-C Lightweight Steels: Research and Prospective. *Metals* **2022**, *12*, 1572. [[CrossRef](#)]
13. Kumar, N.; Singh, K.; Singh, A. Microstructural evolution after heat treatment of high specific strength steel: Fe-13Al-16Mn-5Ni-0.8C and correlation with tensile properties. *Materialia* **2022**, *22*, 101412. [[CrossRef](#)]
14. Ren, P.; Chen, X.P.; Wang, C.Y.; Zhou, Y.X.; Cao, W.Q.; Liu, Q. Evolution of microstructure, texture and mechanical properties of Fe-30Mn-11Al-1.2C low-density steel during cold rolling. *Mater. Charact.* **2021**, *174*, 111013. [[CrossRef](#)]
15. Wang, Z.W.; Lu, W.J.; Zhao, H.; He, J.Y.; Wang, K.; Zhou, B.C.; Ponge, D.; Raabe, D.; Li, Z.M. Formation mechanism of κ -carbides and deformation behavior in Si-alloyed FeMnAlC lightweight steels. *Acta Mater.* **2020**, *198*, 258–270. [[CrossRef](#)]
16. Pang, J.Y.; Zhou, Z.M.; Zhao, Z.Z.; Tang, D.; Liang, J.H.; He, Q. Tensile Behavior and Deformation Mechanism of Fe-Mn-Al-C Low Density Steel with High Strength and High Plasticity. *Metals* **2019**, *9*, 897. [[CrossRef](#)]
17. Ma, L.; Tang, Z.Y.; You, Z.Y.; Guan, G.F.; Ding, H.; Misra, D. Microstructure, Mechanical Properties and Deformation Behavior of Fe-28.7Mn-10.2Al-1.06C High Specific Strength Steel. *Metals* **2022**, *12*, 602. [[CrossRef](#)]
18. Lee, J.W.; Duh, J.G.; Tsai, S.Y. Corrosion resistance and microstructural evaluation of the chromized coating process in a dual phase Fe-Mn-Al-Cr alloy. *Surf. Coat. Technol.* **2002**, *153*, 59–66. [[CrossRef](#)]
19. Lee, J.W.; Wu, C.C.; Liu, T.F. The influence of Cr alloying on microstructures of Fe-Al-Mn-Cr alloys. *Scr. Mater.* **2004**, *50*, 1389–1393. [[CrossRef](#)]
20. Wang, C.S.; Tsai, C.Y.; Chao, C.G.; Liu, T.F. Effect of chromium content on corrosion Behaviors of Fe-9Al-30Mn-(3,5,6,5,8)Cr-1C alloys. *Mater. Trans.* **2007**, *48*, 2973–2977. [[CrossRef](#)]
21. Tuan, Y.H.; Wang, C.S.; Tsai, C.Y.; Chao, C.G.; Liu, T.F. Corrosion behaviors of austenitic Fe-30Mn-7Al-xCr-1C alloys in 3.5% NaCl solution. *Mater. Chem. Phys.* **2009**, *114*, 595–598. [[CrossRef](#)]
22. Tsay, G.D.; Lin, C.L.; Chao, C.G.; Liu, T.F. A New Austenitic FeMnAlCrC Alloy with High-Strength, High-Ductility, and Moderate Corrosion Resistance. *Mater. Trans.* **2010**, *51*, 2318–2321. [[CrossRef](#)]
23. Ren, X.; Li, Y.; Qi, Y.; Wang, C. Effect of Micro-Alloyed/Alloyed Elements on Microstructure and Properties of Fe-Mn-Al-C Lightweight Steel. *Metals* **2022**, *12*, 695. [[CrossRef](#)]
24. Huang, C.F.; Ou, K.L.; Chen, C.S.; Wang, C.H. Research of phase transformation on Fe-8.7Al-28.3Mn-1C-5.5Cr alloy. *J. Alloys Compd.* **2009**, *488*, 246–249. [[CrossRef](#)]
25. Chen, M.S.; Cheng, H.C.; Huang, C.F.; Chao, C.Y.; Qu, K.L.; Yu, C.H. Effects of C and Cr content on high-temperature microstructures of Fe-9Al-30Mn-xC-yCr alloys. *Mater. Charact.* **2010**, *61*, 206–211. [[CrossRef](#)]
26. Kim, K.W.; Park, S.J.; Moon, J.; Jang, J.H.; Ha, H.Y.; Lee, T.H.; Hong, H.U.; Lee, B.H.; Han, H.N.; Lee, Y.J.; et al. Characterization of microstructural evolution in austenitic Fe-Mn-Al-C lightweight steels with Cr content. *Mater. Charact.* **2020**, *170*, 110717. [[CrossRef](#)]
27. Zhang, J.L.; Hu, C.H.; Zhang, Y.H.; Li, J.H.; Song, C.J.; Zhai, Q.J. Microstructures, mechanical properties and deformation of near-rapidly solidified low-density Fe-20Mn-9Al-1.2C-xCr steels. *Mater. Des.* **2020**, *186*, 108307. [[CrossRef](#)]
28. Zhang, J.L.; Liu, Y.X.; Hu, C.H.; Jiang, Y.S.; Addad, A.; Ji, G.; Song, C.J.; Zhai, Q.J. The effect of Cr content on intragranular κ -carbide precipitation in Fe-Mn-Al-(Cr)-C low-density steels: A multiscale investigation. *Mater. Charact.* **2022**, *186*, 111801. [[CrossRef](#)]
29. Liu, J.; Chen, W.P.; Jiang, Z.F.; Liu, L.S.; Fu, Z.Q. Microstructure and mechanical properties of an Fe-20Mn-11Al-1.8C-5Cr alloy prepared by powder metallurgy. *Vacuum* **2017**, *137*, 183–190. [[CrossRef](#)]
30. Liu, M.; Zhou, J.; Zhang, J.; Song, C.; Zhai, Q. Ultra-high strength medium-Mn lightweight steel by dislocation slip band refinement and suppressed intergranular κ -carbide with Cr addition. *Mater. Charact.* **2022**, *190*, 112042. [[CrossRef](#)]
31. Handa, K.; Kimura, Y.; Mishima, Y. Microstructures and Mechanical Properties of the γ/κ Two Phase Fe-Mn-Al-C (-Cr) Alloys. *MRS Online Proc. Libr.* **2000**, *646*, 329–334. [[CrossRef](#)]
32. Yoo, J.D.; Park, K.-T. Microband-induced plasticity in a high Mn-Al-C light steel. *Mater. Sci. Eng.* **2008**, *496*, 417–424. [[CrossRef](#)]
33. Yoo, J.; Hwang, S.; Park, K.-T. Origin of extended tensile ductility of a Fe-28Mn-10Al-1C steel. *Metall. Mater. Trans.* **2009**, *40*, 1520–1523. [[CrossRef](#)]
34. Yang, F.; Song, R.; Li, Y.; Sun, T.; Wang, K. Tensile deformation of low density duplex Fe-Mn-Al-C steel. *Mater. Des.* **2015**, *76*, 32–39. [[CrossRef](#)]
35. Zhang, J.; Jiang, Y.; Zheng, W.; Liu, Y.; Addad, A.; Ji, G.; Song, C.; Zhai, Q. Revisiting the formation mechanism of intragranular κ -carbide in austenite of a Fe-Mn-Al-Cr-C low-density steel. *Scr. Mater.* **2021**, *199*, 113836. [[CrossRef](#)]

36. Wang, H.; Wang, C.; Liang, J.; Godfrey, A.; Wang, Y.; Weng, Y.; Cao, W. Effect of alloying content on microstructure and mechanical properties of Fe–Mn–Al–C low-density steels. *Mater. Sci. Eng.* **2023**, *886*, 145675. [[CrossRef](#)]
37. Moon, J.; Park, S.-J.; Jang, J.H.; Lee, T.-H.; Lee, C.-H.; Hong, H.-U.; Han, H.N.; Lee, J.; Lee, B.H.; Lee, C. Investigations of the microstructure evolution and tensile deformation behavior of austenitic Fe-Mn-Al-C lightweight steels and the effect of Mo addition. *Acta Mater.* **2018**, *147*, 226–235. [[CrossRef](#)]

Disclaimer/Publisher’s Note: The statements, opinions and data contained in all publications are solely those of the individual author(s) and contributor(s) and not of MDPI and/or the editor(s). MDPI and/or the editor(s) disclaim responsibility for any injury to people or property resulting from any ideas, methods, instructions or products referred to in the content.